A Bayesian Network for the Classification of Human Motion as Observed by Distributed Radar

Svenningsson, Peter; Fioranelli, Francesco; Yarovoy, Alexander; Martone, Anthony F.

DOI
10.1109/TAES.2022.3177589

Publication date
2022

Document Version
Final published version

Published in
IEEE Transactions on Aerospace and Electronic Systems

Citation (APA)
Svenningsson, P., Fioranelli, F., Yarovoy, A., & Martone, A. F. (2022). A Bayesian Network for the Classification of Human Motion as Observed by Distributed Radar. *IEEE Transactions on Aerospace and Electronic Systems*, *58*(6), 5661-5674. Article 9780548. https://doi.org/10.1109/TAES.2022.3177589

A Bayesian Network for the Classification of Human Motion as Observed by Distributed Radar

PETER SVENNINGSSON, Member, IEEE
Delft University of Technology, Delft, The Netherlands

FRANCESCO FIORANELLI, Senior Member, IEEE
Delft University of Technology, Delft, The Netherlands

ALEXANDER YAROVOY, Fellow, IEEE
Delft University of Technology, Delft, The Netherlands

ANTHONY F. MARTONE, Senior Member, IEEE
U.S. Army Research Laboratory, Adelphi, MD USA

In this article, a statistical model of human motion as observed by a network of radar sensors is presented where knowledge on the position and heading of the target provides information on the observation conditions of each sensor node. Sequences of motions are estimated from measurements of instantaneous Doppler frequency, which captures informative micromotions exhibited by the human target. A closed-form Bayesian estimation algorithm is presented that jointly estimates the state of the target and its exhibited motion class which are described by a hidden Markov model. To correct errors in the estimated motion class distribution introduced by faulty modeling assumptions, calibration of the probability distribution and measurement likelihood is performed by isotonic regression. It is shown, by modeling sensor observation conditions and by isotonic calibration of the measurement likelihood that a cognitive resource management system is able to increase classification accuracy by 5%–10% while utilizing sensor resources in accordance with defined mission objectives.

Manuscript received 9 October 2021; revised 20 March 2022; released for publication 14 May 2022. Date of publication 24 May 2022; date of current version 6 December 2022.

DOI. No. 10.1109/TAES.2022.3177589

Refereeing of this contribution was handled by G. Hendeby.

This work was supported in part by NWO grant RAD-ART, and in part by the Army Research Laboratory, and was accomplished under Grant W911NF-2020-185.

Authors' addresses: Peter Svenningsson and Alexander Yarovoy are with the Microwave Sensing, Signals and Systems, Delft University of Technology, Delft 2600 AA, The Netherlands, E-mail: (peter.o.svenningsson@gmail.com; a.yarovoy@tudelft.nl); Francesco Fioranelli is Department of Microelectronics, Delft University of Technology, Delft 2628 CD, The Netherlands, E-mail: (f.fioranelli@tudelft.nl); Anthony F. Martone is with U.S. Army Research Laboratory, Adelphi, MD 20783 USA, E-mail: (anthony.f.martone.civ@army.mil). *(Corresponding author: Peter Svenningsson.)*

This work involved human subjects or animals in its research. Approval of all ethical and experimental procedures and protocols was granted by the ethics committee of TU Delft as part of the NWO grant RAD-ART.

NOMENCLATURE

$\bullet_{k\|k-1}$	RV $\bullet$ estimated at time k given all measurements until and including time $k-1$.
$f_{k\|k-1}(\cdot)$	Distribution of $\cdot$ at time k given all measurements until and including time $k-1$.
$\langle \cdot, \cdot \rangle$	Inner product.
$\langle \cdot \rangle$	Mean value of a large number of samples.
y	Random variable defining the motion class, discrete.
ϕ	Random variable defining the aspect angle, discrete.
x	Random variable defining the continuous state parameters of the target, continuous.
$\mathcal{X}$	Set of future radar measurements.

I. INTRODUCTION

Networks of radar sensors can increase the efficacy of perception tasks, such as the tracking and classification of targets by leveraging the diverse observation conditions of the radar nodes. However, the utilization of a sensing network relies on the ability to reliably combine the information from each sensor and potentially manage the radar resources across several tasks. One such application of a radar network is the nonintrusive monitoring of vulnerable individuals to detect a fall or other potentially dangerous events [1]–[3].

Existing literature on the classification of human motion from radar measurements mainly evaluates characterizations of the received signal. Measurements of the Doppler effect from micromotions have been found to have the strong predictive performance [3]–[5]. However, characterizations that incorporate the range response have also been presented [2]. Limitations in these works comprise the following.

1) The orientation of the target relative to the sensor is kept fixed in the experimental environment [3]–[5].
2) Only binary classification in a limited domain is considered [1]–[5].
3) The class variable does not change with time [1]–[5].
4) The method utilizes simulated radar data [6]–[8].

Experimental environments without the abovementioned limitations are here considered to provide naturalistic data, which enables a more accurate understanding of the efficacy of the proposed methods in nonexperimental settings.

Previous work on the classification of naturalistic sequences of human motion observed by a radar network has explored learned representations of sequences by applications of recurrent neural networks [9]. Other work utilizes logistic regression to discriminate between motion classes and defines heuristics for sensor fusion [10]. In contrast,

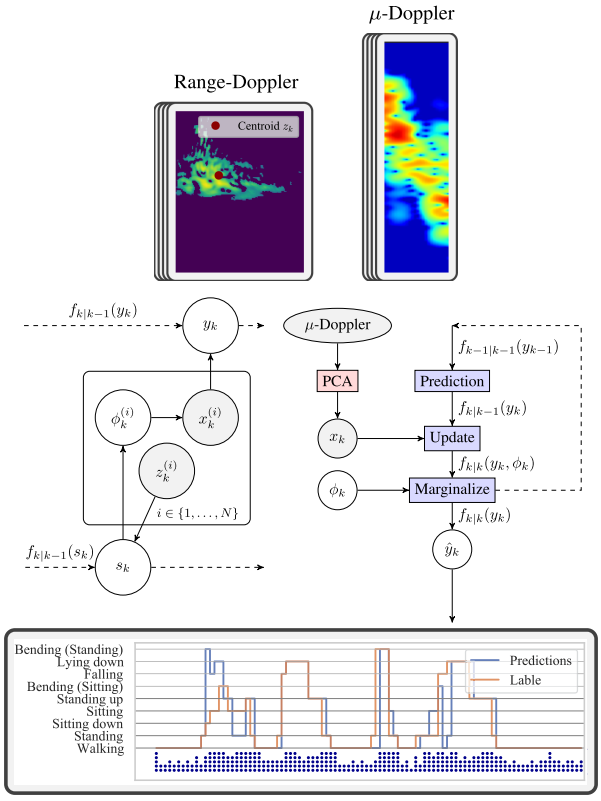

Fig. 1. Diagram of the statistical model and estimation procedure of a radar network monitoring human motion. At time k the marginal distribution of the motion class y_k is evaluated with regards to the observation conditions ϕ_k of each sensing node, which is a deterministic function of the state of the target s_k.

this work proposes a statistical model of human motion that defines a hidden Markov model of a state space, which includes the motion class of the target and the state space of a coordinated turn dynamical model [11]. The classification of human motion is framed as a joint estimation problem where information on the target's position and heading provides an understanding of the observation conditions of each sensor. The proposed statistical model is an acyclic directed graph and can therefore be described as a Bayesian network. An overview of the proposed methodology is visualized in Fig. 1 with notation described in the Nomenclature.

The aim of the presented methodology is not to evaluate a specific characterization of radar measurements as in [1]–[5], [9], [10]. Instead, it is shown how statistical models can be utilized to increase classification performance. In particular, knowledge on variables, which does not directly covary with the motion class is used to increase the information in sensor measurements. Also, it is shown how a model of the dynamical behavior of how a target's motion class is leveraged to differentiate classes that are not separable by the available measurement characterization. In this work such classes are standing, sitting, and lying*down* for which no micromotions can be observed.

Notable related works in Bayesian models for joint estimation problems evaluate how learned representations of Doppler measurements improve data association in simulated environments [12]. In [13], a variational Bayesian method is proposed to reconstruct the instantaneous Doppler frequency from a nonuniform sampling of the radar signal. Other works evaluate classification based on the congruence of a target's motion with defined dynamical models [14], [15]. This work builds on such methods to include the dynamically changing observation conditions of the sensors in a sensing network.

Cognitive radar frameworks rely on an ability to quantify and reason on future uncertainty, which allows for the selection of an optimal decision policy [16], [17]. In previous work on cognitive frameworks for target classification [16], the entropy of the classification variable is used as a proxy for the utility of a measurement, which can be motivated for a single sensor under static observation conditions. Cognitive methods for target classification are here extended to include a model of the observation conditions of each sensing node in a radar network by application of a Monte Carlo approximation of measurement information. As in [16], the aim of the cognitive system is to reduce the utilization of a radar network by taking a set of measurements that are sufficiently informative as defined by some cost function. The resource management problem explored in this work is limited to the selection of micro-Doppler measurements while state point measurements are taken continuously. This restriction is motivated by the long coherent processing interval required by micro-Doppler measurements, which is here considered a dominating factor in measurement cost.

Cognitive radar frameworks and sensor fusion algorithms rely on that the uncertainty estimates provided by the model are meaningful. Poor probability calibration is a consequence of incorrect modeling assumptions, such as the independence of features and the analytical form of estimated distributions [18]. This work proposes the utilization of probability calibration techniques, which improves the performance of the fusion algorithm and increases the reliability of a radar resource management system. Methods of probability calibration are also extended to calibrate measurement likelihood, which is needed to evaluate the information in a radar measurement of the instantaneous frequency spectrum.

In summary, the contributions of this article are as follows:

1) A statistical model of human motion as observed by a network of radar sensors with a closed-form Bayesian estimation algorithm.
2) The solution to a minimal radar network resource problem, which is able to account for the observation conditions of each radar nodes.
3) An extension of probability calibration methods to the proportional calibration of measurement likelihoods.

The signal model is presented in Section II, which outlines the signal processing chain and measurement characterizations followed by the problem formulation in Section III. The proposed statistical model and estimation

procedure are described in Section IV. A resource management problem is defined in Section V, which solution is enabled by the probability calibration technique described in Section VI. Results and the related discussion are found in Sections VII and VIII, respectively, and Section IX concludes this article. For reproducibility, the code has been made available on GitHub[1] and the dataset is published [19].

II. SIGNAL MODEL

A coherently pulsed transceiver transmitting a coded waveform measures the backscatter signal $s : \mathcal{R} \to \mathcal{C}$, which is recovered by a bank of receivers [20]. The in-phase component of $s(t)$ is sampled and the quadrature component is reconstructed by the Hilbert transform [21]. Ranging is inferred from backscatter time-of-flight and the instantaneous frequency spectrum $\hat{s}(t, r, \omega_D)$ is estimated by frequency analysis of the backscatter over a sequence of pulses at a given range r. The spectrum $\hat{s}(t, r, \omega_D)$ describes the Doppler shift of the backscatter. The backscatter can then be characterized by a range-Doppler response where range r and measured radial velocity v_r follow a linear relationship with the time-of-flight τ and Doppler frequency ω_D, respectively,

$$r = \frac{\tau\, c}{2}, \quad v_r = \frac{\lambda\, \omega_D}{2}$$

where λ and c denote the wavelength and the speed of light, respectively.

The instantaneous frequency spectrum $\hat{s}(t, \omega_D)$ of the extended target is estimated by first identifying the frequency f in the bandwidth of $s(t)$ with the highest amplitude. The instantaneous frequency spectrum is then estimated by frequency analysis of f over a sequence of pulses. Frequency analysis has in this work been limited to a discrete Fourier transform of the digitized signal with parameters found in Table I. The instantaneous frequency spectrum can be visualized as a spectrogram that describes the micro-Doppler signature of the target which is found in Fig. 2.

A low dimensional representation of the micro-Doppler spectrogram is acquired by principal component analysis (PCA). A dataset $X \in R^{n \times k}$ is constructed by drawing n samples of one-second duration from the recorded micro-Doppler spectrograms where k denotes the number of elements in a micro-Doppler sample. PCA finds a linear and orthogonal basis $P \in R^{k,\tilde{k}}$, which comprise an optimal low-rank approximation of the covariance matrix of $X \in R^{n,k}$ [22]. The information retained in the $\tilde{k}$ dimensional representation of the micro-Doppler spectrograms

$$\tilde{X} = XP$$

can be visualized by the reconstruction $\hat{X} = \tilde{X}P^T$. PCA as a method for low-rank approximations of micro-Doppler spectra to be used in classification has been established

TABLE I
Experimental Parameters

The class set		
Walking	Standing	Bending (standing)
Sitting down	Sitting	Bending (sitting)
Standing up	Falling	Lying down
Dataset		
Total data recorded		900 min
Naturalistic data recorded		60 min
Number of participants		14 individuals
Sensor and signal processing		
Range resolution	ΔR	9.153 mm
Surveillance area		1–5.39 m
Doppler resolution	$\Delta\omega_D$	1.91 Hz, 0.069 m s^{-1}
Unambiguous Doppler frequency		$\pm$61 Hz, $\pm$2.2 m s^{-1}
Center frequency	λ	4.3 GHz
Pulse repetition frequency	f_{PRF}	122 Hz
Doppler FFT window length		64 pulses, 0.525 s
Average transmit power		50 μW
Antenna Beam Pattern		Omnidirectional
Estimation		
Number of sensors	N	5 sensors
Number of detections at time k	$\hat{N}_k$	5 detections
Num. μ-Doppler meas. at time k	$\tilde{N}_k$	5 Spectrograms
Aspect angle bins	M	8 bins
Spectrogram sample width		1 s
Number of principal components	$\tilde{n}$	20
Time discretization	T	0.5 s
Monte-Carlo samples	$\lvert S\rvert$, N_{mc}	10^4 samples
Measurement noise	σ_r, $\sigma_{\dot{r}}$	0.45 m, 0.45 m s^{-1}
Process noise	σ_v, $\sigma_{\dot{\phi}}$	1 m s^{-1}, 15° s^{-1}

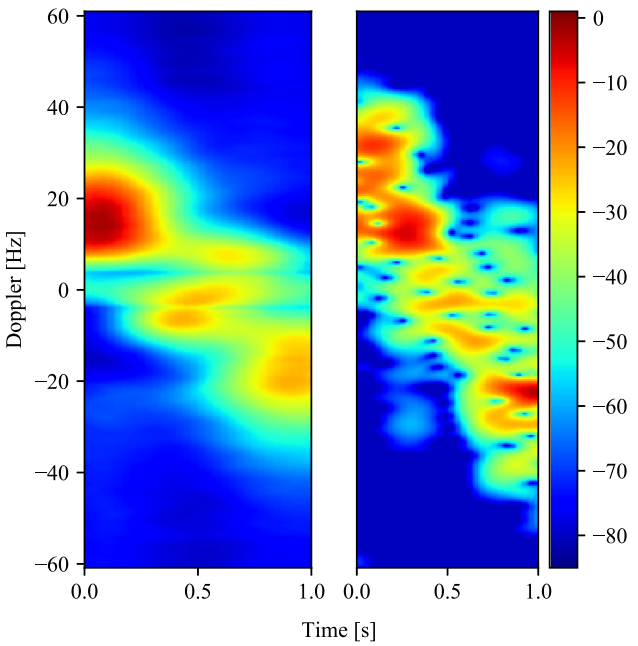

Fig. 2. Micro-Doppler sample of a walking motion (right) and its reconstruction from 20 principal components (left). The spectrograms are visualized in logarithmic scale (dB) relative to the largest amplitude.

[1][Online]. Avaialable: https://github.com/petersvenningsson/radar-Bayesian-human-motion

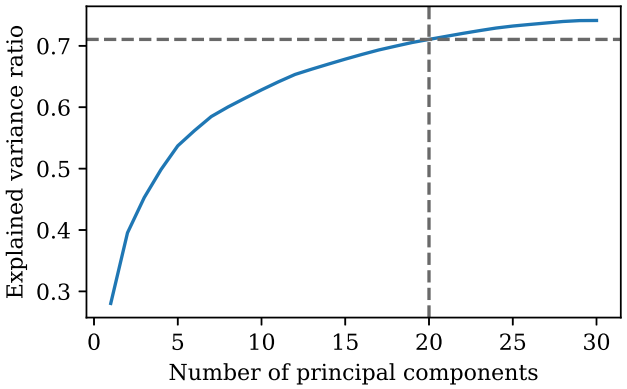

Fig. 3. Explained variance ratio is the proportion of the total variance in the dataset explained by a given number of principal components. It is a metric on the quality of the low-rank approximation. The explained variance ratio of the 20 first principal components is 0.710%.

in the literature [23]–[29], and is here further motivated by the visual similarity between the spectrogram X and its reconstruction $\hat{X}$, which is found in Fig. 2. Following the recommendation in [30], the number of principal components is set so that the proportion of the total variance in the dataset explained by the low-rank approximation exceeds 70%, which occurs at $\tilde{k} = 20$. The choice of $\tilde{k}$ is further motivated by the decreasing improvements in explained variance for a larger number of principal components than the set value as seen in Fig. 3.

Before fitting the PCA transform, the micro-Doppler samples are shifted along the frequency axis to align the amplitude centroid of $\hat{s}(t, \omega_D)$ with zero-Doppler, postprocessing aimed at making the samples directly comparable by hiding information related to the velocity of the target. To account for differences in the amplitude of the backscatter which decreases with the fourth power of the range to the target, the micro-Doppler samples are evaluated in decibels relative to the highest amplitude over a four-second interval. The duration of the interval was found to be appropriate by visual inspection. The dynamic range is set to the interval $[-80, 1]$ dB. The dataset used to fit the PCA transform is subsampled to uniform class distribution to account for class imbalance.

The space complexity of an exact PCA implementation is $\mathcal{O}(n\,k)$. Due to the large dataset used in this work, an approximate PCA algorithm [31] with space complexity $\mathcal{O}(k)$ is used where memory requirements are lowered by processing the dataset in batches.

III. PROBLEM FORMULATION

A surveillance area is observed by five monostatic pulsed radar nodes. The surveillance area is inscribed by a circle with diameter 4.39 m, as shown in Fig. 4. One human target is present in the surveillance area and at each time step exhibits one of nine motion classes found in Table I. For two minutes, the target exhibits a sequence of motion classes considered a facsimile of naturalistic data. Correlations over long periods of time exist in the data. For example, a target may stand up only after sitting down or falling over.

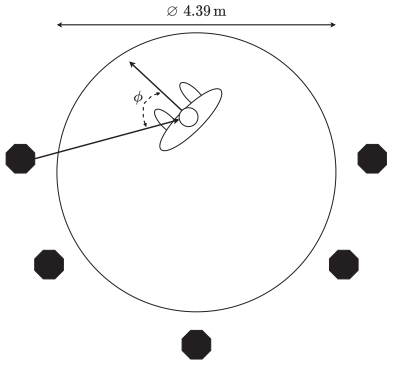

Fig. 4. Surveillance area is visualized with the placement of the radar nodes ⬣ and the aspect angle ϕ of a radar node.

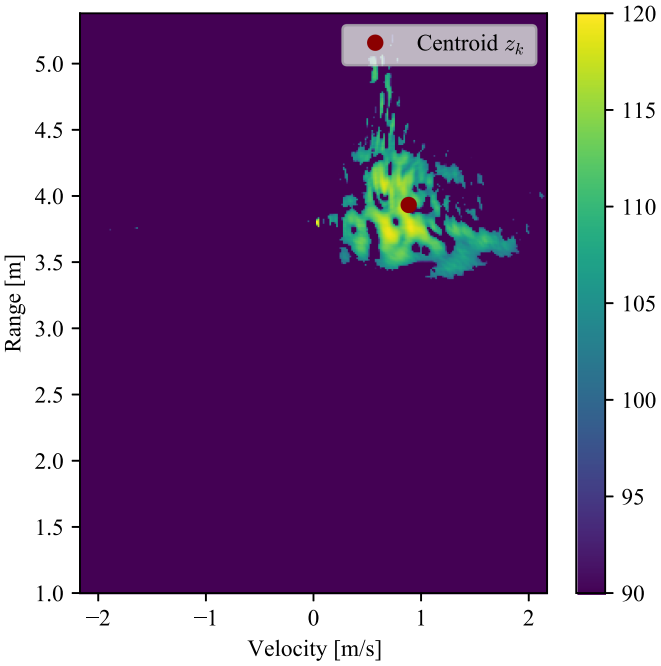

Fig. 5. Range-Doppler response of a human target. The response is truncated to zero at the 80% percentile to remove thermal noise and low amplitude clutter. Visualized in logarithmic scale (dB).

The experimental configuration of the PulsON P410 radar system used in this work is found in Table I. The target extends in range and Doppler is identified by truncating the amplitude of the response to zero at the 80% percentile. The range-Doppler response of a human target is shown in Fig. 5. The amplitude centroid of the truncated response z_k is defined as a point measurement of the target

$$z_k = \left[\frac{\sum_{r,\omega_D} r \,\mathrm{trunc}\,(\hat{s}(t_k, r, \omega_D))}{\sum_{r,\omega_D} \mathrm{trunc}\,(\hat{s}(t_k, r, \omega_D))}, \ldots \right. \\ \left. \frac{\sum_{r,\omega_D} \omega_D \,\mathrm{trunc}\,(\hat{s}(t_k, r, \omega_D))}{\sum_{r,\omega_D} \mathrm{trunc}\,(\hat{s}(t_k, r, \omega_D))} \right] \quad (1)$$

with truncation defined as

$$\mathrm{trunc}(x) = \begin{cases} x & \text{if } x > 0.8 \max(\hat{s}(t_k, r, \omega_D)) \\ 0 & \text{else} \end{cases}.$$

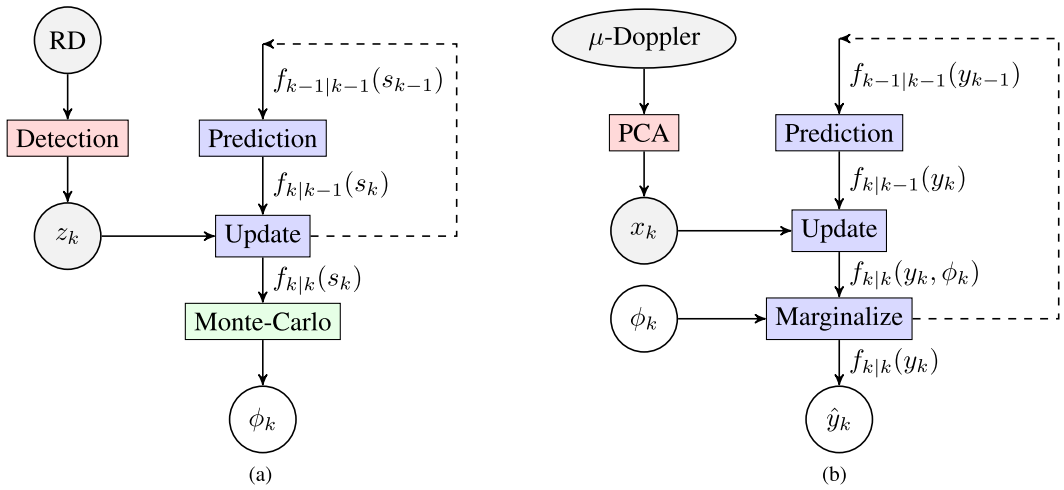

Fig. 6. Overview of the estimation procedure for target state and motion class. The observation conditions of each sensor is estimated in (a) by Monte Carlo sampling. In the motion class estimation procedure shown in (b) distribution of y is updated based the conditional measurement likelihood $p(x_k \mid y_k, \phi_k)$ after which the marginal distribution of y_k is taken. (a) The estimation procedure for the target state s_k and sensor aspect angle ϕ_k. (b) The estimation procedure for the motion class y.

At each time-step t_k a detection is generated from each sensor.

An algorithm is tasked with predicting the exhibited motion class for each time step in the sequence comprising a semantic segmentation in time. The algorithm's performance is characterized by the total accuracy of the predictions and the macroaveraged Jaccard index. Total accuracy is defined as

$$\text{Total accuracy} = \frac{\text{Correct predictions}}{\text{Number of predictions}}$$

and measures the classification performance disregarding class imbalance. The Jaccard index [32]

$$J = \frac{\text{TP}}{\text{TP} + \text{FP} + \text{FN}}$$

is evaluated for each class as a function of the true positives (TP), false positives (FP), and false negatives (FN). The mean Jaccard index is taken over the classes, which constitutes the macroaveraged Jaccard index J_{ma}.

IV. STATISTICAL MODEL

The motion class of the target is estimated from a low-dimensional representation x of micro-Doppler spectrograms one second in duration acquired by principal components decomposition. The response of x covaries with the motion class of the target as well as the observation conditions of the sensor. The observation conditions are modeled in order to increase the information in $x \mid \phi$ relative to the motion class y. The observation conditions here considered is the aspect angle ϕ as visualized in Fig. 4.

The target state and motion class are estimated jointly by the recursive filtering algorithm outlined in Fig. 6 and explained throughout the remaining section. It is assumed that the sensors take independent measurements and that any conditional distribution of x is a multivariate normal distribution with a diagonal correlation matrix. A graphical model of the system is found in Fig. 8.

A. State Estimation

An overview of the state estimation algorithm is found in Fig. 6(a). The aim of the state estimation algorithm is to map a sequence of sets of point measurements to a sequence of estimates of the aspect angle ϕ_k for each sensor

$$Z_0, Z_1, \ldots, Z_k \quad \mapsto \quad \Phi_{0|0}, \Phi_{1|1}, \ldots, \Phi_{k|k}$$

where $Z_0 = \{z^{(1)}, \ldots, z^{(\hat{N}_k)}\}$, $\Phi = \left\{\phi^{(1)}, \ldots, \phi^{(N)}\right\}$, for N sensors and $\hat{N}_k$ detections at time k.

The state of the target s_{k-1} is mapped to the next time step s_k by a deterministic process model $g_k(\cdot)$ with additive Gaussian noise

$$s_k = g_k(s_{k-1}) + q_k, \quad q_k \sim \mathcal{N}(0, Q_k)$$

where Q_k denotes the covariance matrix of the noise. A sensor is modeled by a deterministic measurement model $h_k(s_k)$ with Gaussian noise

$$z_k = h_k(s_k) + r_k, \quad r_k \sim \mathcal{N}(0, R_k)$$

where R_k denotes the covariance matrix of the noise.

The recursive estimation of s_k can then be decomposed into the Chapman–Kolmogorov prediction

$$f_{k|k-1}(s_k) = \int g\big(s_k \mid s_{k-1}\big) f_{k-1|k-1}\big(s_{k-1}\big) \mathrm{d}s_{k-1} \qquad (2)$$

and update step following from Bayes rule

$$f_{k|k}(s_k) \propto h(Z_k \mid s_k) f_{k|k-1}(s_k) \qquad (3)$$

for which there exists closed form solutions if $g(\cdot)$ and $h(\cdot)$ are linear functions and the noise is additive Gaussian [33].

The target's state vector $s = [x_1, x_2, v, \varphi, \dot{\varphi}]$ defines the position, velocity, heading, and turn rate of the target. It is

assumed that the target follows a coordinated turn process model, which is discretized by the Euler method [11]

$$g(s) = \begin{bmatrix} x_1 + T v \cos(\phi) \\ x_2 + T v \sin(\phi) \\ v \\ \varphi + T\dot{\varphi} \\ \dot{\varphi} \end{bmatrix} \tag{4}$$

with time-step length T and noise covariance

$$Q = \operatorname{diag}\left(\begin{bmatrix} 0 & 0 & \sigma_v^2 & 0 & \sigma_{\dot{\phi}}^2 \end{bmatrix}\right).$$

The radar nodes in the sensing network take point measurements of range and radial velocity as modeled by

$$h(s) = \begin{bmatrix} \|x - b\| \\ \left\langle \begin{bmatrix} v\cos\varphi \\ v\sin\varphi \end{bmatrix}, x - b \right\rangle \end{bmatrix} \tag{5}$$

with noise covariance

$$R = \operatorname{diag}\left(\begin{bmatrix} \sigma_r^2 & \sigma_{\dot{r}}^2 \end{bmatrix}\right)$$

where $x = [\, x_1 \; x_2 \,]^T$ denotes the position of the target and $b = [\, b_1 \; b_2 \,]^T$ the position of the sensor.

The nonlinear process model (4) and measurement model (5) are linearized around $s_{k-1|k-1}$ and $s_{k|k-1}$, respectively. This approximation is commonly referred to as extended Kalman filtering [33].

The aspect angle ϕ from a sensor to the target follow the deterministic relationship

$$\Gamma(s) = \operatorname{arctan2}(b_2 - x_2, b_1 - x_1) - \operatorname{mod}(\varphi, 2\pi).$$

The aspect angle ϕ is estimated by a Monte Carlo approximation. Let $\mathcal{S}$ be a set of samples drawn from $s_{k|k}$. The aspect angle ϕ is discretized into M equisized bins and is estimated by

$$P\left(\phi = \phi^{(j)}\right) = \frac{\sum_{s\in\mathcal{S}} \mathbf{1}_{[j-\frac{2\pi}{M}, j+\frac{2\pi}{M}]}(\Gamma(s))}{|\mathcal{S}|}$$
$$j \in \{0, \ldots (M-1)\}$$

where $\mathbf{1}$ is the indicator function.

B. Class Estimation

The motion class exhibited by the target is modeled as a discrete Markov chain, which is visualized in Fig. 7. An overview of the estimation procedure for the motion class is found in Algorithm 6b.

The distribution of the motion class y is estimated recursively. The discrete process model

$$f_{k|k-1}(y_k) = Q\, y_{k-1}$$

maps the motion class y at time $k-1$ to the succeeding time step k. The transition matrix $Q \in \mathbf{R}^{M\times M}$ defines the transition between M classes where $Q_{np} = P(y_k = n \mid y_{k-1} = p)$.

The conditional distribution of $x_k^{(i)} \mid y_k$ is modeled as Gaussian with a diagonal covariance matrix Σ

$$p(x_k \mid y_k) \sim \mathcal{N}(x_k;\, \mu,\, \Sigma)$$

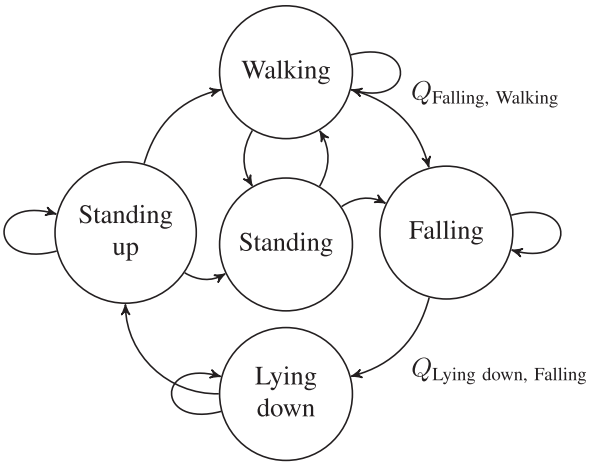

Fig. 7. First-order Markov model of a subset of the motion classes which defines $f_{k|k-1}(y_k)$.

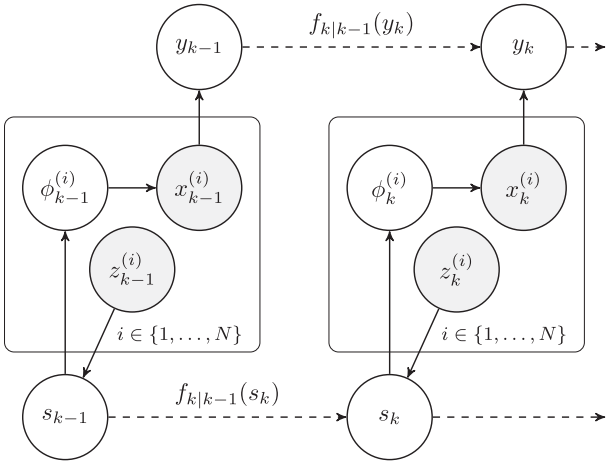

Fig. 8. Graphical model of the target and sensor network, which can be categorized as a dynamic Bayesian network. The state s_k and motion class y_k are estimated dynamically from range-Doppler point measurements $x_k^{(i)}$ and micro-Doppler measurements $z_k^{(i)}$. The sensors in the radar network, which are modeled as independent, are indexed by i. Shading indicates variables that are directly observed.

where

$$f_{k|k}(y_k) \propto p(x_k \mid y_k)\, f_{k|k-1}(y_k).$$

Similarly, the observation conditions ϕ are considered by assuming

$$p\left(x_k \mid y_k, \phi_k\right) \sim \mathcal{N}(x_k;\, \mu,\, \Sigma)$$

where an estimate of $f_{k|k}(y_k)$ is obtained by its marginal distribution

$$f_{k|k}(y_k) \propto \sum_{\phi} p\left(x_k \mid y, \phi\right)\, f_{k|k}\left(\phi_k\right)\, f_{k|k-1}(y_k).$$

For a network of multiple sensors, the Bayesian network shown in Fig. 8 is factorized by

$$f_{k|k}(y_k) \propto \sum_i \sum_{\phi_k^{(i)}} p\left(x_k^{(i)} \mid y, \phi_k^{(i)}\right)\, f_{k|k}\left(\phi_k^{(i)}\right)\, f_{k|k-1}(y_k) \tag{6}$$

where $i \in \{1, \ldots, \bar{N}_k\}$ and $\bar{N}_k$ denotes the number of valid measurements of x_k at time k. A micro-Doppler measurement may be considered invalid if the target leaves the sensing node's line-of-sight during the coherent processing interval. In this work, $\bar{N}_k = N$ for all k.

The parameters of the distributions, $p(x_k \mid y_k)$ and $p(x_k \mid y_k, \phi_k)$ are estimated from data with known labels y and point estimates of ϕ are extracted from Algorithm 6a.

V. RESOURCE MANAGEMENT

Resource management can be viewed as a decision process where the utility of an action accounts for the cost of the action and the expected benefits associated with the action. A minimal resource management problem is here formulated as

$$\max_{\mathcal{X}_{k+1}} \; \mathrm{I}\left(\mathcal{X}_{k+1}; y_{k+1|k}\right) - c\,|\mathcal{X}_{k+1}| \quad \text{For } \mathcal{X}_{k+1} \text{ over } \mathcal{P}(\mathcal{S}) \tag{7}$$

where $\mathcal{X}$ is the set of selected radar sensors, $\mathcal{P}$ denotes all subsets of $\mathcal{S}$, and $\mathcal{S} = \left\{x_{k+1}^{(1)} \mid \phi_{k+1}^{(1)}, \ldots, x_{k+1}^{(N)} \mid \phi_{k+1}^{(N)}\right\}$ is the set of available sensors with corresponding observation conditions $\phi_{k+1}^{(i)}$. The utility function in (7) weighs the information in a set of future measurements $\mathrm{I}(\mathcal{X}_{k+1}; y_{k+1})$ against the cost of the using $|\mathcal{X}_{k+1}|$ number of sensors as defined by the cost factor c.

The information in a future measurement is quantified as the conditional information in $x_{k+1} \mid \phi_{k+1|k}$ relative to the motion class $y_{k+1\,|\,k}$

$$\mathrm{I}\left(x_{k+1} \mid \phi_{k+1|k}; y_{k+1|k}\right) = \mathbb{E}_{p(x,y,\phi)} \log \frac{p(x, y \mid \phi)}{p(x \mid \phi)\, p(y \mid \phi)} \tag{8}$$

where time indices have been dropped from the notation for brevity. Considering a set of independent sensors $\mathcal{X}_{k+1} = \left\{x^{(1)} \mid \phi^{(1)}, \ldots, x^{(N)} \mid \phi^{(N)}\right\}$ with corresponding angle estimates $\Phi_{k+1|k}$ the information in a measurement from the sensors in $\mathcal{X}$

$$\mathrm{I}(\mathcal{X}; y) = \mathbb{E}_{p(\mathcal{X},y,\Phi)} \log \frac{p(\mathcal{X}, y)}{p(\mathcal{X})\, p(y)} \tag{9}$$

can be expressed in the conditional form

$$\mathrm{I}(\mathcal{X}; y) = \mathbb{E}_{p(\mathcal{X},y,\Phi)} \log \frac{p(\mathcal{X} \mid y)}{\sum_y' p(\mathcal{X} \mid y')\, p(y')}$$

and

$$\mathrm{I}(\mathcal{X}; y) = \mathbb{E}_{p(\mathcal{X},y,\Phi)} \log \frac{\prod_{x^{(i)} \in \mathcal{X}} p(x^{(i)} \mid \phi^{(i)}, y)}{\sum_y' \prod_{x^{(i)} \in \mathcal{X}} p(x^{(i)} \mid \phi^{(i)}, y')\, p(y')} \tag{10}$$

follows from the independence of the sensors in $\mathcal{X}$. The conditional distributions $p\left(x^{(i)} \mid \phi^{(i)}, y\right)$ are modelled as Gaussian and the expectation in (10) is approximated by Monte Carlo sampling

$$\mathrm{I}(\mathcal{X}; y) = \mathbb{E}_{p(\mathcal{X},y,\Phi)} \log \frac{p(\mathcal{X} \mid y)}{\sum_y' p(\mathcal{X} \mid y')\, p(y')} \approx \left\langle \log \frac{\prod_{x^{(i)} \in \mathcal{X}} p(x^{(i)} \mid \phi^{(i)}, y)}{\sum_y' \prod_{x^{(i)} \in \mathcal{X}} p(x^{(i)} \mid \phi^{(i)}, y')\, p(y')} \right\rangle \tag{11}$$

over N_{mc} samples which are drawn with replacement from the training split. Information is here and throughout the manuscript defined in base e.

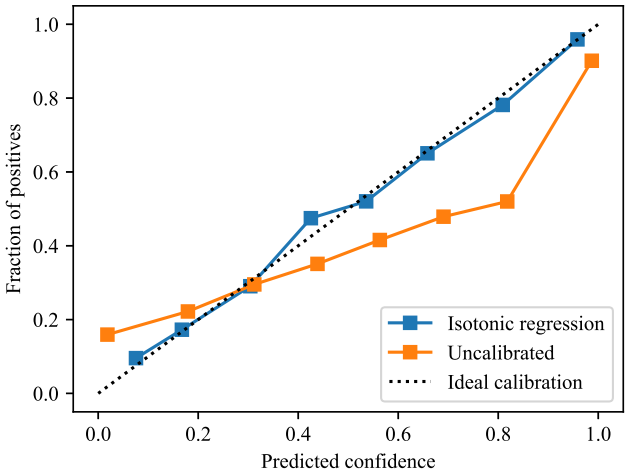

Fig. 9. Reliability curve for the binary prediction if the target is exhibiting the *Walking* motion class. The classification is made on a uniform prior with no dynamical modeling of the human motion. The uncalibrated classification model is overconfident and the isotonic calibration method is able to correct the confidence of the predictions.

VI. MODEL CALIBRATION

Methods that aim to correct the predicted class probability $\hat{y}$ to make it more similar to the true class probability y are named probability calibration methods [18]. The aim is for a prediction made at confidence q to have the probability q of being true. A well-calibrated model improves the efficacy of data fusion over time and across sensors as uncertainty estimates remain meaningful. The calibration of a classification model can be characterized by a reliability curve which is found in Fig. 9.

Following the method proposed by [34], a function m is fit to minimize the squared error of predictions made on a validation dataset $\mathcal{V}$

$$\hat{m} = \mathrm{argmin}_m \sum_{i \in \mathcal{V}} \left(y_i - m\left(\hat{y}_i\right)\right)^2 \tag{12}$$

where y_i denotes an annotated motion class and $\hat{y}_i$ is the respective prediction. The function $\hat{m}$ is restricted to a piecewise constant monotonically increasing function and is fit using the pair-adjacent violators algorithm [35] developed for isotonic regression. The validation dataset $\mathcal{V}$ is generated by folded validation.

This work extends probability calibration to the proportional calibration of measurement likelihoods. Let the motion class y be estimated from the measurement of one

sensor $x \in \mathbb{R}^{\hat{k}}$ using a uniform prior $\bar{p}(y)$

$$\hat{p}(y) = \frac{p(x \mid y)\,\bar{p}(y)}{\sum_y' p(x \mid y)\bar{p}(y)}.$$

The distribution of $\hat{p}(y)$ is calibrated on a uniform prior by subsampling the validation dataset $\mathcal{V}$ to a uniform class distribution. The calibrated measurement likelihood can then be approximated as

$$\hat{m}\big(\hat{p}(y)\big) \approx \frac{p(x \mid y)\,\bar{p}(y)}{\sum_{y'} p(x \mid y')\bar{p}(y')} = \frac{p(x \mid y)}{\sum_{y'} p(x \mid y')} \tag{13}$$

where

$$\frac{p(x \mid y)}{\sum_{y'} p(x \mid y')} \propto p(x \mid y).$$

The calibrated measurement likelihood are used in the motion class estimation update step (6)

$$f_{k|k}(y_k) \propto \sum_i \sum_{\phi_k^{(i)}} \hat{m}\left(\hat{p}\left(y \mid x_k^{(i)}, \phi_k^{(i)}\right)\right)$$
$$f_{k|k}\left(\phi_k^{(i)}\right)\ f_{k|k-1}(y_k)$$

and to estimate the information in a measurement from a set of sensors (10)

$$\mathrm{I}(\mathcal{X}; y) = \mathbb{E}_{p(\mathcal{X},y,\Phi)} \log \frac{\prod_{x^{(i)} \in \mathcal{X}} \hat{m}\left(\hat{p}\left(y \mid x^{(i)}, \phi^{(i)}\right)\right)}{\sum_y' \prod_{x^{(i)} \in \mathcal{X}} \hat{m}\left(\hat{p}\left(y' \mid x^{(i)}, \phi^{(i)}\right)\right) p(y')}.$$

The calibrated measurement likelihood has been optimized to reflect how well the measurements can discriminate between the classes and can, therefore, more accurately estimate how much information exists in a measurement. The calibrated measurement likelihood also improves the outcome of sensor fusion as uncertainty in the measurements is more correctly estimated.

VII. CASE STUDY

A human target exhibiting a sequence of motion classes has been recorded in an experimental environment described in Section II and visualized in Fig. 4. A total of 900min of data has been recorded, of which 60 min are naturalistic data sequences. The predictive model proposed in Section IV is evaluated on naturalistic data sequences using folded validation where a test fold comprises data from an individual not found in the training fold. The parameters of the conditional distributions $p(x \mid y, \phi)$ are estimated from the training fold from a maximum *a posteriori* probability point estimate of ϕ. The calibration procedure splits the training fold into an additional five folds to estimate the model's probability predictions on test data. Parameters related to the dataset and the estimation procedure are found in Table I.

The performance of the proposed model is evaluated by an ablation study. The effects of different components of the proposed solution are analyzed by observing the decrease in the performance when removed. The components evaluated by the ablation study are as follows:

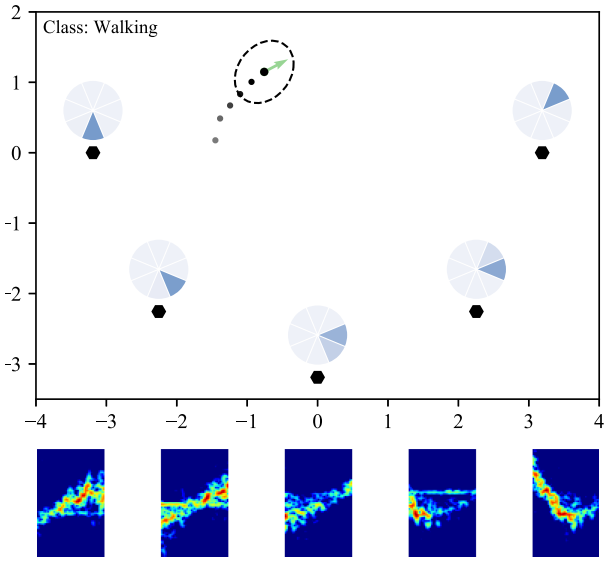

Fig. 10. Radar nodes ⬣ visualized with the estimated aspect angle to the target ⊕ where the shading indicates the probability mass of the discrete aspect angles. The 3-sigma bound of the target's position is indicated by - - -. The measurement noise σ_r, $\sigma_{\dot{r}}$ has been tuned so that the 3-sigma bound approximates the cross-section of the target. The instantaneously Doppler frequency measured by each sensor is visualized on the bottom row. Video renderings of the track are available at https://bit.ly/3jMy9Cm.

1) A dynamic estimation of the motion class.
2) An estimation of the observation conditions of the radar nodes.
3) A calibration of the model's uncertainty estimates.

When all three components are missing the statistical model is a Gaussian naive Bayes classifier.

A. Results

A visualization of the state estimation track is found in Fig. 10. The algorithm tracks the position of the target with a 3-sigma bound of approximately 0.7 m. Each sensor's estimated discrete aspect angle can be estimated with high certainty when the target is in motion. However, if the target remains stationary, the uncertainty in the aspect angle is high. Rendered videos of the target track have been made available at https://bit.ly/3jMy9Cm.

The ablation study found in Table II verifies that each component of the statistical model increases classification performance by 2%–6% accuracy. The proposed solution achieves an accuracy of 64.9% and a Jaccard index of 31.1%. In contrast, the simplest model which is equivalent to a Gaussian naive Bayes classifier, achieves an achieves of 54.6%, and a Jaccard index of 24.3%.

The confusion matrix found in Fig. 11 shows that the model has high accuracy for predictions made on the Walking class, which has a steady-state micro-Doppler signature. Contrary, the model has low performance for predictions made on motion classes with short complex micromotions, such as falling, sitting down, and bending.

TABLE II
Comparison of Classification Performance When Components of the Proposed Method Are Not Included in the Estimation Procedure

Observation conditions	Uncalibrated	Calibrated
Dynamic estimation		
Accuracy		
Conditioned on ϕ	61.9 %	**64.9 %**
Not conditioned on ϕ	59.4 %	62.4 %
Jaccard index		
Conditioned on ϕ	29.1 %	**31.1 %**
Not conditioned on ϕ	27.3 %	28.4 %
Static estimation [a]		
Accuracy		
Conditioned on ϕ	56.8 %	58.4 %
Not conditioned on ϕ	54.6 %	55.8 %
Jaccard index		
Conditioned on ϕ	25.6 %	26.3 %
Not conditioned on ϕ	24.3 %	24.8 %

[a] A prediction for each sample is estimated without fusion over time. Fusion over the five sensors follows from Bayes rule with a uniform prior. The three components of the proposed method, dynamic estimation of the motion class, conditioning the measurements on observation conditions and calibration of the measurement likelihood increases accuracy by 6.5%, 2.5%, and 3.0% respectively.
The highest values in the table are set as bold to be more easily found.

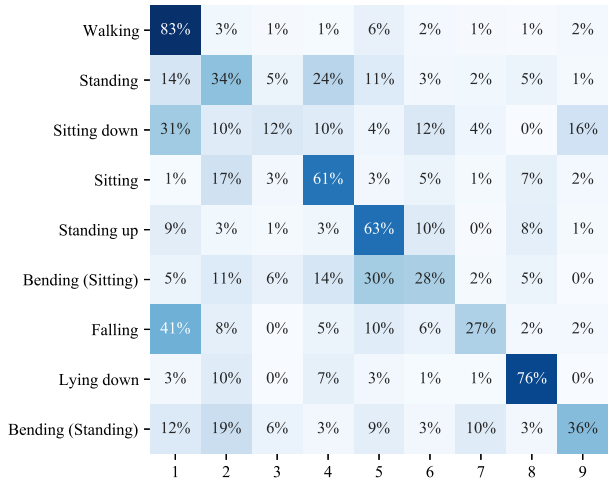

Fig. 11. Confusion matrix of predictions made by the proposed model. True labels are indicated on the y-axis and predicted labels on the x-axis. Shown values are normalized by the number of true samples.

The classes standing, sitting, and lying down are motionless and are not separable by their micro-Doppler signature. The model can separate these classes by leveraging information on the transition between classes as encoded in the transitions matrix Q. The accuracies for lying down and sitting are 76 and 61%, respectively, while standing is predicted with lower accuracy of 34% and is misclassified as Sitting at a rate of 24%, which shows a difficulty in identifying the transition between these classes. The model also shows some confusion between the nonstationary Walking class and the stationary motion classes, which indicates that information on the target's velocity has been obfuscated by the postprocessing of the micro-Doppler samples.

TABLE III
Breakdown of the Information in a Single Calibrated Measurement Taken at Different Aspect Angles

Aspect angle bin j [a]	Information	Accuracy [b]
Conditioned on ϕ		
$j = 0$	**0.79**	**50.5 %**
$j = 1$	0.73	43.0 %
$j = 2$	0.61	37.4 %
$j = 3$	0.72	45.2 %
$j = 4$	0.71	50.4 %
$j = 5$	0.65	47.7 %
$j = 6$	0.61	33.4 %
$j = 7$	0.71	45.1 %
Not conditioned on ϕ		
$j = 0$	0.61	47.9 %
$j = 1$	0.61	40.6 %
$j = 2$	0.61	32.7 %
$j = 3$	0.61	42.5 %
$j = 4$	0.61	46.8 %
$j = 5$	0.61	45.4 %
$j = 6$	0.61	28.8 %
$j = 7$	0.61	41.9 %

[a] The aspect angle interval $[\frac{2j-\pi}{8}\ \frac{2j+\pi}{8}]$.
[b] A prediction is here estimated independently without fusion over time or across sensors.
In the operational domain, higher accuracy is achieved at inference from measurement near aspect angles $\phi' \in \{0, \pi\}$ corresponding to aspect angle bins $j \in \{0, 4\}$. When the observation conditions are modeled, the increased information at ϕ' can be identified.

A breakdown of the information in micro-Doppler measurements at varying observation conditions is found in Table III. Measurements are most informative at angle bins 0 and 4, which signifies that the target is measured from the front and back, respectively. Many micromotions such as swinging arms can be measured well under these observation conditions. Prediction accuracy from measurements taken at different observation conditions follows the trends of measurement information with predictions made at aspect angle bins 0 and 4 being the most accurate. The information in measurements from the most advantageous observation conditions is 0.79 nats while the information in the least advantageous observation conditions is 0.61 nats, which is coincidentally also the information in measurements where the observation conditions have not been modeled. A upper bound on the measurement information is $\log(9) \approx 2.20\,nats$, which is the logarithm of the size of the class set [36]. Significant decreases in measurement information and classification performance are found if observation conditions are not modeled.

The predictions of a cognitive system classifying a motion sequence while managing sensor resources by solving the resource management problem expressed in (7) are visualized in Fig. 12. Fewer measurements are taken when the model has high certainty on the motion class, such as during long sequences of walking. At times of high uncertainty such as when the information in measurements is conflicting or ambiguous, an increased number of measurements are taken. The advantages of taking more measurements are

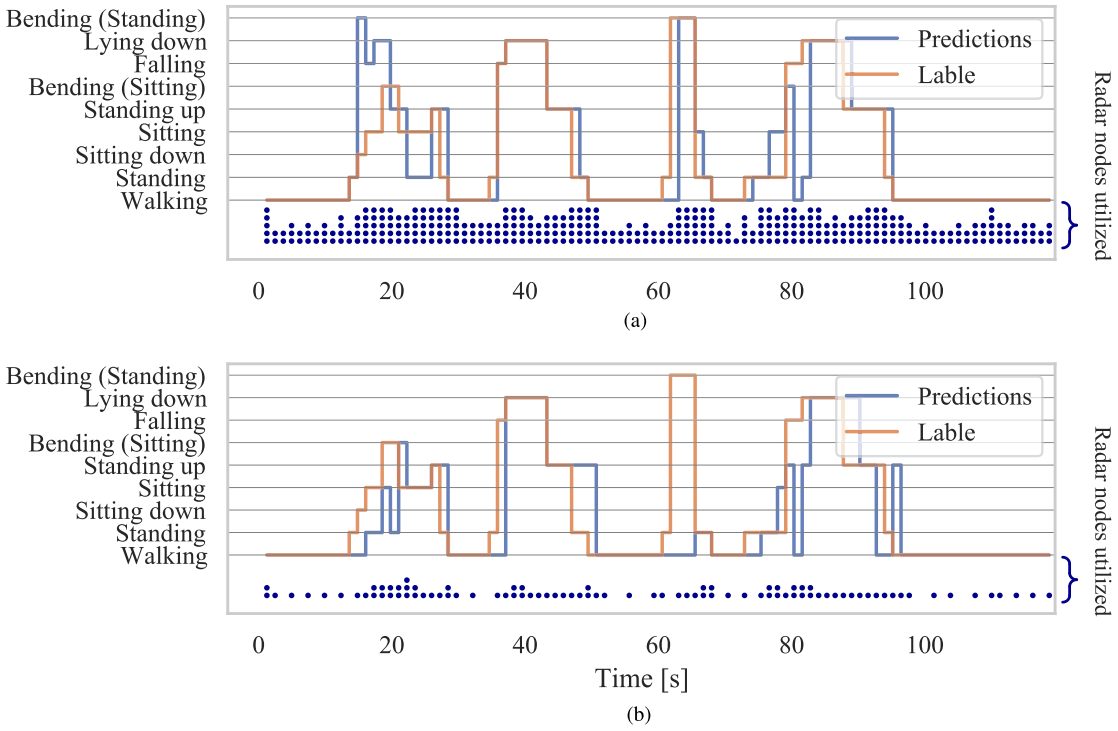

Fig. 12. Classification predictions made by a cognitive system which selects the set of radar measurements to take in order to maximize the utility in (7). (a) Low measurement cost scenario $c = 0.04$. (b) High measurement cost scenario $c = 0.4$.

made clear as the low measurement cost scenario shown in Fig. 12(a) is able to classify the Bending motion at 60 s which is misclassified in the high-cost scenario shown in Fig. 12(b).

Quantitative results on resource management are found in Fig. 13. The classification performance increases with sensor utilization, defined as the ratio of utilized micro-Doppler measurements over the total number of possible measurements available. Resource management systems that use a statistical model that includes sensor observation conditions performs well at 20–40% sensor utilization as these systems can select the sensors with the most informative measurements based on the current observation conditions—outperforming simpler statistical models by 3–5% in the interval.

At sensor utilization higher than 20% the calibrated models outperform uncalibrated models by 2.5–4% as the efficacy of sensor fusion is improved by calibration. As shown in Fig. 13(b), the uncalibrated models also systematically under- and overutilize sensor resources as the information in the measurements is overestimated. It is assumed that the calibrated model utilizes sensor resources correctly because its uncertainty estimates are well-calibrated, as shown in Fig. 9.

VIII. DISCUSSION

The results in Secion VII show that increased measurement information and classification performance is achieved by modeling sensor observation conditions. As seen in Table III modeling the observation conditions improves the predictive performance and measurement information across all evaluated aspect angles. As radar sensors only measure velocity in the radial direction, the micro-Doppler signature may vary significantly with the aspect angle. Consequently, by conditioning on the observation conditions the model can expect an reduced micro-Doppler response from a disadvantageous aspect angle and make predictions accordingly. This behavior can be seen in Table III as significant increases in the performance are found for the aspect angle bins 2 and 6 in which the micro-Doppler response is likely to be reduced for the motion classes explored in this work.

By modeling the observation conditions, an increase of 3 percentiles in accuracy is achieved, as shown in Table II. Since information on the aspect angle of the target is only available when the point object model of the target is in motion, this increase in the performance is isolated to the walking and a subset of the samples in the falling class. Future work includes the validation of the proposed method on an experimental dataset that comprises a diverse set of classes where the target is in motion and consequently information on the aspect angle available. Examples of such classes are walking, limping, and crawling.

The importance of modeling the observation conditions of the sensor network is supported by the increases in the performance of cognitive systems in high measurement cost scenarios. Knowledge on the observation conditions enables a cognitive system to select the most favorable

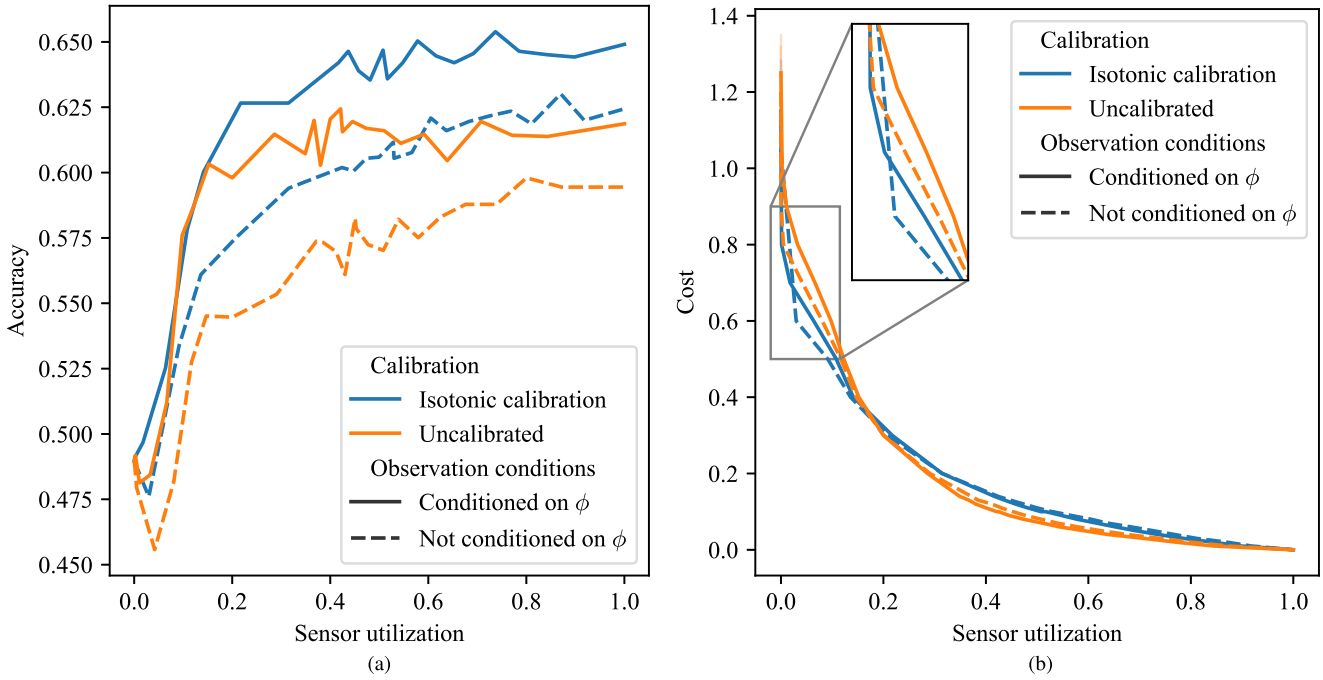

Fig. 13. Resource management results from a cognitive system operating under statistical models of varying complexity. Sensor utilization is defined as $\frac{\text{total measurements taken}}{\text{total measurements available}}$. (a) Proposed method of a calibrated statistical model which includes sensor observation conditions has the strongest classification performance. The network utilization determined by the cognitive system for a given cost function is visualized (b) which shows that uncalibrated models may over- or underutilize sensor resources. Note the qualifying legend where ▬ indicates that isotonic calibration is used and the prediction is conditioned on the observation conditions ϕ. (a) Classification performance. (b) Resource management decision making.

sensors, which leads to an increase in the performance at a given rate of sensor utilization. These models of observation conditions could be extended according to mission requirements to include other variables, such as signal-to-noise ratio, waveform parameters, and the possibility of interference.

Uncertainty estimates provided by calibrated models are shown in Fig. 9 to have high reliability while the uncalibrated model is overconfident. The performance increases in sensor fusion outcomes that should follow from calibration are confirmed by the increases in classification accuracy in Table II. This performance increase is partly caused by better utilization of the information stored in the motion class transition matrix as the classification prior is incorrectly disregarded if the model has poor probability calibration.

Model calibration also impacts the cognitive system, which manages the sensor resources. If the model is poorly calibrated, the measurement information estimated by (11) will not be meaningful. Consequently, the uncalibrated model overutilizes the sensor resources for high measurement cost as the cognitive system overestimates how well observations of x separates the motion classes. For low measurements cost the uncalibrated system underutilizes sensor resources as the entropy of y is underestimated. In both these situations, the cognitive system is operating contrary to mission goals. Hence, model calibration increases the reliability of cognitive systems.

Information on the velocity of the target was obfuscated in the postprocessing procedure described in Section II to make the recorded micromotions more directly comparable across samples. However, in the classification predictions shown in Fig. 11 there exists confusion between stationary and nonstationary classes that should be separable by the target's velocity. The tracked velocity of the target may be included as a classification covariate to distinguish these classes but was not explored in this article in order to reduce the systematic complexity of the proposed method.

Only one target is present in the surveillance area in the experimental setup used in this work. This assumption allows for a simple signal processing chain used to estimate the instantaneous frequency Doppler spectrum disseminated by the target. However, it is not a realistic assumption for practical applications. If multiple targets are present in the surveillance area, then a detector and tracking algorithm with support for multiple targets can be used to localize the targets. The instantaneous time Doppler frequency for any given target can then be estimated by frequency analysis of the range bin where the target is located. If the targets are not separable in range then hardware that allows for beamforming could be used, e.g., MIMO array FMCW radars. The implementation of one such signal processing chain to estimate the instantaneous Doppler frequency spectrum of multiple targets is presented in [37].

This article has explored how modeling observation conditions in a sensing network can increase performance

under the operation of a cognitive resource management system in the application of classification of human motion from micro-Doppler measurements. The application space was suitable to validate the methodology because micro-Doppler varies strongly with sensor aspect angle as some motions may give a severely reduced Doppler response under disadvantageous observation conditions. However, the proposed method generalizes to other applications, such as the classification of fixed-wing aircraft from characterizations of radar cross-section, which vary with sensor aspect angle [38]. The investigation of more application domains as well as the exploration of more diverse and possibly multimodal sets of classification covariates constitutes topics for future work.

IX. CONCLUSION

A statistical model has been presented, which incorporates sensor observation conditions into the classification of human motion from measurements of micromotions. The marginalization over observation conditions and the calibration of measurement likelihoods are two novel components of the estimation procedure validated by an ablation study as the removal of either of these components is detrimental to performance. An increase of 2 and 3 percentiles in accuracy and Jaccard index is achieved by modeling the sensor observation conditions and calibrating the measurement likelihoods, respectively.

A cognitive system has been proposed which solves a minimal resource management problem which comprises the selection of sensors to observe the future micromotions of the target. The system can utilize knowledge on sensor observation conditions to improve its ability to satisfy defined objectives. In addition, it has been shown how probability calibration procedures can be used to increase the reliability of cognitive systems so that resources are utilized in accordance with user-defined cost functions. Knowledge on observation conditions and calibrations procedures have been shown to increase the classification accuracy of the cognitive system 5%–10% for varying measurement costs scenarios.

ACKNOWLEDGMENT

The views and conclusions contained in this document are those of the authors and should not be interpreted as representing the official policies, either expressed or implied, of the Army Research Laboratory or the U.S. Government. The U.S. Government is authorized to reproduce and distribute reprints for Government purposes notwithstanding any copyright notation herein. The authors are grateful to R. Guendel and all the participants in the data collection.

REFERENCES

[1] B. Jokanović and M. Amin
Fall detection using deep learning in range-doppler radars
IEEE Trans. Aerosp. Electron. Syst., vol. 54, no. 1, pp. 180–189, Feb. 2017.

[2] B. Erol and M. G. Amin
Radar data cube analysis for fall detection
in *Proc. IEEE Int. Conf. Acoust. Speech Signal Process.*, 2018, pp. 2446–2450.

[3] M. G. Amin, Y. D. Zhang, F. Ahmad, and K. D. Ho
Radar signal processing for elderly fall detection: The future for in-home monitoring
IEEE Signal Process. Mag., vol. 33, no. 2, pp. 71–80, Mar. 2016.

[4] B. Erol, M. Amin, F. Ahmad, and B. Boashash
Radar fall detectors: A comparison
in *Proc. Int. Soc. Opt. Photon.*, 2016, Art. no. 982918.

[5] D. P. Fairchild and R. M. Narayanan
Classification of human motions using empirical mode decomposition of human micro-Doppler signatures
IET Radar, Sonar Navigat., vol. 8, no. 5, pp. 425–434, 2014.

[6] Y. Lang, Q. Wang, Y. Yang, C. Hou, D. Huang, and W. Xiang
Unsupervised domain adaptation for micro-Doppler human motion classification via feature fusion
IEEE Geosci. Remote Sens. Lett., vol. 16, no. 3, pp. 392–396, Mar. 2019.

[7] H. Du, Y. He, and T. Jin
Transfer learning for human activities classification using micro-Doppler spectrograms
in *Proc. IEEE Int. Conf. Comput. Electromagn.*, 2018, pp. 1–3.

[8] I. Bilik and J. Tabrikian
Radar target classification using doppler signatures of human locomotion models
IEEE Trans. Aerosp. Electron. Syst., vol. 43, no. 4, pp. 1510–1522, Oct. 2007.

[9] P. Chen *et al.*
Multi-view real-time human motion recognition based on ensemble learning
IEEE Sensors J., vol. 21, no. 18, pp. 20335–20347, Sep. 2021.

[10] R. G. Guendel, M. Unterhorst, E. Gambi, F. Fioranelli, and A. Yarovoy
Continuous human activity recognition for arbitrary directions with distributed radars
in *Proc. IEEE Radar Conf.*, 2021, pp. 1–6.

[11] M. Roth, G. Hendeby, and F. Gustafsson
EKF/UKF maneuvering target tracking using coordinated turn models with polar/cartesian velocity
in *Proc. 17th Int. Conf. Inf. Fusion*, 2014, pp. 1–8.

[12] A. Dubey, A. Santra, J. Fuchs, M. Lübke, R. Weigel, and F. Lurz
A Bayesian framework for integrated deep metric learning and tracking of vulnerable road users using automotive radars
IEEE Access, vol. 9, pp. 68758–68777, 2021.

[13] K. Ren, L. Du, B. Wang, Q. Li, and J. Chen
Statistical compressive sensing and feature extraction of time-frequency spectrum from narrowband radar
IEEE Trans. Aerosp. Electron. Syst., vol. 56, no. 1, pp. 326–342, Feb. 2020.

[14] M. Li and Z. Jing
Multi-target joint detection, tracking and classification based on generalized Bayesian risk using radar and ESM sensors
2018, *arXiv:1807.02267*.

[15] B. Ristic and P. Smets
Target classification approach based on the belief function theory
IEEE Trans. Aerosp. Electron. Syst., vol. 41, no. 2, pp. 574–583, Apr. 2005.

[16] K. Bell, G. Smith, A. Mitchell, and M. Rangaswamy
Multiple task hierarchical fully adaptive radar
in *Proc. 52nd Asilomar Conf. Signals, Syst., Comput.*, 2018, pp. 1344–1348.

[17] M. I. Schöpe, H. Driessen, and A. Yarovoy
Multi-task sensor resource balancing using lagrangian relaxation and policy rollout
in *Proc. IEEE 23rd Int. Conf. Inf. Fusion*, 2020, pp. 1–8.

[18] A. Niculescu-Mizil and R. Caruana
Predicting good probabilities with supervised learning
in *Proc. 22nd Int. Conf. Mach. Learn.*, 2005, pp. 625–632.

[19] R. G. Guendel, M. Unterhorst, F. Fioranelli, and A. Yarovoy
Dataset of continuous human activities performed in arbitrary directions collected with a distributed radar network of five nodes
Nov. 2021. [Online]. Available: https://data.4tu.nl/articles/dataset/Dataset_of_continuous_human_activities_performed_in_arbitrary_directions_collected_with_a_distributed_radar_network_of_five_nodes/16691500/2

[20] Multirate filter banks
in *Multirate and Wavelet Signal Processing (Wavelet Analysis and Its Applications)*, vol. 8, B. W. Suter, Ed. New York, NY, USA: Academic, 1998, ch. 3, pp. 73–143.

[21] R. N. Bracewell and R. N. Bracewell
The Fourier Transform and Its Applications, vol. 31999, New York, NY, USA: McGraw-Hill, 1986.

[22] J. Shlens
A tutorial on principal component analysis
2014, *arXiv:1404.1100*.

[23] K. Saho, M. Fujimoto, M. Masugi, and L.-S. Chou
Gait classification of young adults, elderly non-fallers, and elderly fallers using micro-doppler radar signals: Simulation study
IEEE Sensors J., vol. 17, no. 8, pp. 2320–2321, Apr. 2017.

[24] J. Zabalza, C. Clemente, G. Di Caterina, J. Ren, J. J. Soraghan, and S. Marshall
Robust PCA micro-doppler classification using SVM on embedded systems
IEEE Trans. Aerosp. Electron. Syst., vol. 50, no. 3, pp. 2304–2310, Jul. 2014.

[25] L. Zhu, S. Zhang, Q. Ma, H. Zhao, S. Chen, and D. Wei
Classification of UAV-to-ground targets based on enhanced micro-Doppler features extracted via PCA and compressed sensing
IEEE Sensors J., vol. 20, no. 23, pp. 14360–14368, Dec. 2020.

[26] B. Erol, S. Z. Gurbuz, and M. G. Amin
Motion classification using kinematically sifted ACGAN-synthesized radar micro-Doppler signatures
IEEE Trans. Aerosp. Electron. Syst., vol. 56, no. 4, pp. 3197–3213, Aug. 2020.

[27] B. Erol and M. G. Amin
Radar data cube processing for human activity recognition using multisubspace learning
IEEE Trans. Aerosp. Electron. Syst., vol. 55, no. 6, pp. 3617–3628, Dec. 2019.

[28] X. Qiao, M. G. Amin, T. Shan, Z. Zeng, and R. Tao
Human activity classification based on micro-Doppler signatures separation
IEEE Trans. Geosci. Remote Sens., vol. 60, 2021, Art. no. 5105014.

[29] I. Choi, K. Kang, K. Kim, and S. Park
Use of ICA to separate micro-Doppler signatures in ISAR images of aircraft that has fast-rotating parts
IEEE Trans. Aerosp. Electron. Syst., vol. 58, no. 1, pp. 234–246, Feb. 2022.

[30] I. T. Jolliffe and J. Cadima
Principal component analysis: A review and recent developments
Philos. Trans. Roy. Soc. A: Math., Phys. Eng. Sci., vol. 374, no. 2065, 2016, Art. no. 20150202.

[31] D. A. Ross, J. Lim, R.-S. Lin, and M.-H. Yang
Incremental learning for robust visual tracking
Int. J. Comput. Vis., vol. 77, no. 1, pp. 125–141, 2008.

[32] P. Jaccard
The distribution of the flora in the alpine zone
1," *New Phytologist*, vol. 11, no. 2, pp. 37–50, 1912.

[33] S. Särkkä
Bayesian Filtering and Smoothing, no. 3, Cambridge, MA, USA:Cambridge Univ. Press, 2013.

[34] B. Zadrozny and C. Elkan
Transforming classifier scores into accurate multiclass probability estimates
in *Proc. 8th ACM SIGKDD Int. Conf. Knowl. Discov. Data Mining*, 2002, pp. 694–699.

[35] M. Ayer, H. D. Brunk, G. M. Ewing, W. T. Reid, and E. Silverman
An empirical distribution function for sampling with incomplete information
Ann. Math. Statist., pp. 641–647, 1955.

[36] T. M. Cover and J. A. Thomas
Elements of Information Theory (Telecommunications and Signal Processing). New York, NY, USA: Wiley-Interscience, 2006.

[37] S. Zhu
Multiple target tracking and human activity recognition based on the IR-UWB radar sensor networks
Master's thesis, Delft University of Technology, Delft, The Netherlands, 2021. [Online]. Available: http://resolver.tudelft.nl/uuid:8a0a66cc-7d94-4149-aa56-4213a588b86d

[38] S. Chen, K. Yue, B. Hu, and R. Guo
Numerical simulation on the radar cross section of variable-sweep wing aircraft
J. Aerosp. Technol. Manage., vol. 7, pp. 170–178, 2015.

Peter Svenningsson (Member, IEEE) received the B.Sc. degree in engineering mathematics, the B.Sc. degree in mechanical engineering, and the M.Sc. degree in engineering mathematics from the Chalmers University of Technology, Gothenburg, Sweden, all three degrees formally awarded in 2020.

October 2020, he joined the Microwave Sensing, Signals and Systems Group, Delft University, Delft, The Netherlands, as a Ph.D. candidate and to work on cognitive radar perception systems. In August 2021, he joined the Emerging Business Department, Husqvarna Group to develop perception and localization solutions for autonomous systems.

Francesco Fioranelli (Senior Member, IEEE) received the Ph.D. degree in electronic engineering from Durham University, Durham, U.K., in 2014.

He is currently an Assistant Professor with Delft University of Technology, Delft, The Netherlands, and was an Assistant Professor with the University of Glasgow (2016–2019), and a Research Associate with University College London, London, U.K. (2014–2016). His research interests include the development of radar systems and automatic classification for human signatures analysis in healthcare and security, drones and UAVs detection and classification, automotive radar, wind farm, and sea clutter.

Alexander Yarovoy (Fellow, IEEE) received the Diploma (Hons.) degree in radiophysics and electronics from Kharkov State University, Kharkiv, Ukraine, in 1984 and the Candidate Physics and Mathematical Sciences and Doctor Physics and Mathematical Sciences degrees in radiophysics from Kharkiv State University, Ukraine, in 1987 and 1994, respectively.

In 1987, he joined the Department of Radiophysics, Kharkov State University as a Researcher and became a Full Professor in 1997. From September 1994 to 1996, he was with Technical University of Ilmenau, Ilmenau, Germany, as a Visiting Researcher. Since 1999, he is with the Delft University of Technology, Delft, The Netherlands. Since 2009, he leads there a Chair of Microwave Sensing, Systems and Signals. His main research interests are in high-resolution radar, microwave imaging and applied electromagnetics (in particular, UWB antennas). He has authored and coauthored more than 450 scientific or technical papers, six patents, and 14 book chapters.

Dr. Yarovoy is the recipient of the European Microwave Week Radar Award for the paper that best advances the state-of-the-art in radar technology in 2001 (together with L.P. Ligthart and P. Van Genderen) and in 2012 (together with T. Savelyev). In 2010 together with D. Caratelli Prof. Yarovoy was the recipient of the best paper award of the Applied Computational Electromagnetic Society (ACES). He was the General TPC Chair of the 2020 European Microwave Week (EuMW'20), was the Chair and the TPC Chair of the 5th European Radar Conference (EuRAD'08), as well as the Secretary of the 1st European Radar Conference (EuRAD'04). He was the Co-Chair and TPC Chair of the Xth International Conference on GPR (GPR2004). He was an Associated Editor for the *International Journal of Microwave and Wireless Technologies* from 2011 to 2018 and as a Guest Editor of five special issues of the IEEE Transactions and other journals. In the period 2008–2017, he was the Director of the European Microwave Association (EuMA).

Anthony F. Martone (Senior Member, IEEE) received the B.S. (*summa cum laude*) degree in electrical engineering from Rensselaer Polytechnic Institute, Troy, NY, USA, in 2001 and the Ph.D. degree in electrical engineering from Purdue University, West Lafayette, IN, USA, in 2007.

He joined the U.S. Army Research Laboratory, Adelphi, MD, USA, in 2007 as a Researcher in the RF Signal Processing and Modeling branch where his research interests include sensing through the wall technology, spectrum sharing, and radar signal processing. He is currently the Sensors and Electron Devices Directorate lead for Cognitive Radar research where he is overseeing, directing, and collaborating with multiple universities to address spectrum sharing for radar and communication systems, software-defined transceiver control, and adaptive processing techniques. He was a committee member for graduate students with The Pennsylvania State University, State College, PA, USA, the Virginia Polytechnic Institute and State University, Blacksburg, VA, USA, and Bowie State University, Bowie, MD, USA. Since joining ARL, he has authored more than 100 journal and conference publications, two book chapters, and ten patents.

Dr. Martone is an Associate Editor for the IEEE TRANSACTIONS ON AEROSPACE AND ELECTRONIC SYSTEMS since 2017. He was the recipient of the Commanders Award for Civilian Service in December 2011 for his research and development of sensing through the wall signal processing techniques. Recently, he was nominated to the IEEE Aerospace and Electronic Systems Society Radar Systems Panel in October 2019 where he serves on the Spectral Innovations and Publications Committees.